The Population of Pulsating Variable Stars in the Sextans Dwarf Spheroidal Galaxy

A. Katherina Vivas 10, Javier Alonso-García 2,30, Mario Mateo 4, Alistair Walker 10, and Brittany Howard 1 Cerro Tololo Inter-American Observatory, National Optical Astronomy Observatories, Casilla 603, La Serena, Chile; kvivas@ctio.noao.edu 2 Centro de Astronomía (CITEVA), Universidad de Antofagasta, Av. Angamos 601, Antofagasta, Chile 3 Instituto Milenio de Astrofísica, Santiago, Chile 4 Department of Astronomy, University of Michigan, Ann Arbor, MI 48109, USA

Department of Astronomy, University of Michigan, Ann Arbor, MI 48109, USA

Department of Physics and Astronomy, University of Victoria, P.O. Box 1700 STN CSC, Victoria, BC V8W 2Y2, Canada Received 2018 September 13; revised 2018 November 26; accepted 2018 November 28; published 2019 January 4

Abstract

A large extension of the Sextans dwarf spheroidal galaxy, 7 deg², has been surveyed for variable stars using the Dark Energy Camera at the Blanco Telescope at Cerro Tololo Inter-American Observatory, Chile. We report seven anomalous Cepheids, 199 RR Lyrae stars, and 16 dwarf Cepheids in the field. This is only the fifth extragalactic system in which dwarf Cepheids have been systematically searched. Henceforth, the new stars increase the census of stars coming from different environments that can be used to asses the advantages and limitations of using dwarf Cepheids as standard candles in populations for which the metallicity is not necessarily known. The dwarf Cepheids found in Sextans have a mean period of 0.066 day and a mean g amplitude of 0.87 mag. They are located below the horizontal branch, spanning a range of 0.8 mag: 21.9 < g < 22.7. The number of dwarf Cepheids in Sextans is low compared with other galaxies such as Carina, which has a strong intermediate-age population. On the other hand, the number and ratio of RR Lyrae stars to dwarf Cepheids are quite similar to those of Sculptor, a galaxy which, as Sextans, is dominated by an old stellar population. The dwarf Cepheid stars found in Sextans follow a well-constrained period-luminosity relationship with an rms = 0.05 mag in the g band, which was set up by anchoring to the distance modulus given by the RR Lyrae stars. Although the majority of the variable stars in Sextans are located toward the center of the galaxy, we have found two RR Lyrae stars and one anomalous Cepheid in the outskirts of the galaxy that may be extratidal stars and suggest that this galaxy may be undergoing tidal destruction. These possible extratidal variable stars share the same proper motions as Sextans, as seen by recent Gaia measurements. Two additional stars that we initially classified as foreground RR Lyrae stars may actually be other examples of Sextans extratidal anomalous Cepheids, although radial velocities are needed to prove that scenario.

Key words: galaxies: dwarf – galaxies: individual (Sextans) – galaxies: stellar content – stars: variables: general – stars: variables: RR Lyrae

Supporting material: figure set, machine-readable table

1. Introduction

Below the horizontal branch (HB), an interesting group of pulsating variable stars can be found. These stars, named δ Scuti (Sct) if metal-rich and SX Phoenicis (Phe) if metalpoor, have an important property: they follow a periodluminosity (PL) relationship (Sandage & Tammann 2006; McNamara 2011 and reference therein) and thus could be used, in principle, as standard candles with a precision similar to that of RR Lyrae stars (\sim 5%–7%). These stars can also be numerous. The Large Magellanic Cloud (LMC), for example, contains a couple thousand of them (Garg et al. 2010; Poleski et al. 2010), while the Carina dwarf spheroidal (dSph) galaxy has \sim 400, about 5 times the number of RR Lyrae stars in that galaxy (Vivas & Mateo 2013; Coppola et al. 2015). In the LSST era, these pulsating stars will be found to large distances and motivate further study of their properties to understand their use and limitations as extragalactic standard candles and tracers of structure within the halo of the Milky Way.

The naming of the δ Sct and SX Phe types of variable stars has not been without controversy in the past (see Catelan & Smith 2015 for an extensive discussion). In this paper, we will use the term dwarf Cepheid (DC) to refer collectively to the high-amplitude δ Sct (HADS) stars and the SX Phe variables (following other works such as Mateo 1993 and Vivas & Mateo 2013). The reasoning behind the use of this nomenclature

is that both stars occupy the same region in the Hertzsprung–Russell (H-R) diagram, and, because dSph galaxies can contain a mix of stellar populations, it is not easy to know if, in these systems, those variable stars belong to Population I (hence, if they are δ Sct stars), Population II (hence, if they are SX Phe stars), or a mix of both. Furthermore, both types of stars share similar pulsational characteristics (Balona & Nemec 2012), and, particularly important in the context of this work, they seem to share the same PL relationship (Cohen & Sarajedini 2012). On the other hand, the evolutionary status of HADS and SX Phe stars could not be more different. The HADS stars are thought to be main-sequence stars that lie within the instability strip, while SX Phe stars are blue stragglers (BSs) from old populations and have reached that position in the H-R diagram through binary evolution.

Cohen & Sarajedini (2012) suggested that the PL relationship of DCs does not depend on color or metallicity. Their PL relationship was constructed by joining DC stars from galactic globular clusters and a few extragalactic systems (the LMC, Fornax, and a small sample from Carina known at the time of that work); that is, it contains both HADS and SX Phe stars. The dispersion in the resulting PL relation is relatively large, ~0.1 mag, although the authors claimed that part of the scatter may be due to calibration differences between the multiple data sets used in their work. In any case, it is an encouraging result

that these stars may be used as distance indicators even for systems or populations for which the metallicity is not known. However, more systems with DC stars coming from different environments (age, metallicity, star formation history) are needed in order to confirm the general use of such a PL relationship. In this respect, the dSph galaxies contain stars that inhabit a different age/metallicity range than found anywhere else in the Galaxy and so offer the chance to study DCs (and other variables) from unique and otherwise hard-to-study populations.

A previous study in Carina (Vivas & Mateo 2013) has raised several interesting points. (i) Carina is very rich in DC stars. It has the highest specific frequency of DCs among the other extragalactic systems and the globular clusters of the Milky Way. (ii) There seems to be a fundamental difference between the DC population in dSph galaxies and the galactic field. While high-amplitude DCs are extremely rare in the field (Balona & Nemec 2012), they are at least 100× more frequent in Carina. (iii) There are important differences observed among the properties of the DC population of Carina, Fornax, and the LMC that may be a reflection of a metallicity spread, depth along the line of sight, and/or different evolutionary paths of the DCs.

In this work, we search for DC stars in another of the dSph galaxies around the Milky Way, Sextans. Our main goal is characterize the DC population in this galaxy and increase the number of such stars in extragalactic systems. We will defer the derivation of a unique PL relationship for a future paper once other galaxies in our program have been surveyed.

Sextans is a low-luminosity system located 86 kpc from the Sun, similar to the distance to Carina. But, contrary to Carina, it has an older population and a much lower surface brightness. It does not have a strong intermediate-age population, although there is evidence of continuous star formation in the last \sim 8 Gyr (Lee et al. 2009) and a significant spread in metallicity (Battaglia et al. 2011). Numerous stars in the BS region have been observed in Sextans (Mateo et al. 1991, 1995; Lee et al. 2009). These are the stars that are located in the instability strip and may be pulsating as DCs. The search for variable stars in Sextans has been limited in the past due in part to its large extension in the sky (its tidal radius is $\sim 83'-120'$; Irwin & Hatzidimitriou 1995; Roderick et al. 2016; Okamoto et al. 2017; Cicuéndez et al. 2018). Prior to this study, no DC stars were known in this galaxy, and even the census of brighter variable stars such as RR Lyrae stars was incomplete (Mateo et al. 1995; Amigo 2012; Medina et al. 2018). Here we take advantage of the large field of view (FoV) of the Dark Energy Camera (DECam; Flaugher et al. 2015) to search for variable stars in a large extension of the Sextans dSph.

This paper is structured as follow. In Section 2, we describe the observational strategy to find DC stars in Sextans and discuss the methods used for reducing the data and obtaining photometry. We search for variable stars in Section 3. Although the focus of this work is the DC stars, other types of pulsating stars, such as RR Lyrae stars and anomalous Cepheids, were also found and characterized. The large spatial coverage in our survey allows us to explore the existence of possible extratidal variables in Sextans (Section 4). The distance to Sextans from its RR Lyrae stars is derived in Section 5. Then, in Section 6, we derive a PL relationship for DC stars in Sextans by anchoring to the distance modulus obtained by the RR Lyrae stars. Finally, we discuss and compare the properties of DC stars in Sextans with the ones known in other extragalactic systems in Section 7. Concluding remarks are given in Section 8.

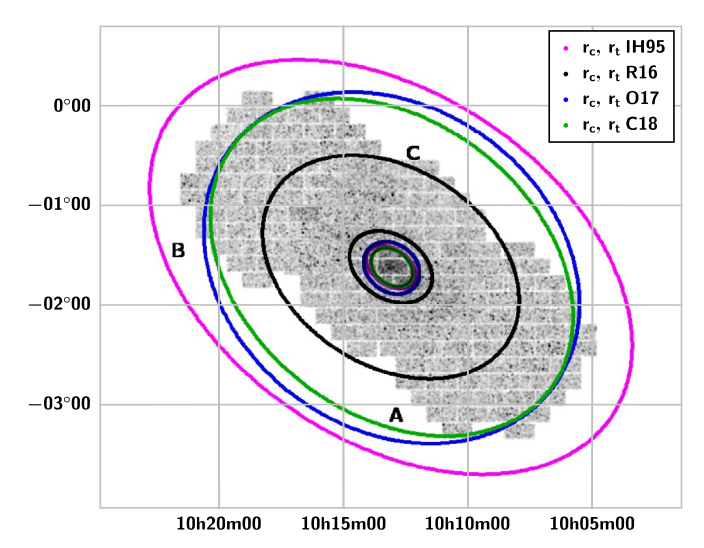


Figure 1. Density map in equatorial coordinates of objects detected in the three fields observed with DECam, labeled A, B, and C (Table 1). The ellipses with different colors indicate the King's core radius (r_c) and tidal radius (r_t) determined by Irwin & Hatzidimitriou (1995; magenta), Roderick et al. (2016; black), Okamoto et al. (2017; blue), and Cicuéndez et al. (2018; green).

2. Observations

The DC stars are faint pulsating stars located in the instability strip, ~ 1.5 –2.5 mag below the HB. Since the Sextans HB is located at $g \sim 20.5$, we expect the Sextans DC stars to have magnitudes g between 22 and 23. The other important property of DC stars necessary for planning the observational campaign is their pulsational periods. They have very short periods, $\lesssim 0.1$ day, with a peak close to 0.06 day, or 1.4 hr (Breger 2000). In consequence, for distant systems such as Sextans, medium/large-aperture telescopes are required, since exposure times should be kept short so that they do not cover a significant fraction of the pulsation period.

DECam is an ideal instrument to pursue a survey of DC stars in Sextans. Not only does it have a large FoV (3 deg²), it is also installed on a 4 m telescope, the Blanco Telescope at Cerro Tololo Inter-American Observatory, Chile. We observed three fields with DECam that cover a large extension of the galaxy (Figure 1). The determination of the size of the Sextans galaxy has been quite controversial. In Figure 1, we show the location of the observed DECam fields together with the King's core radius (r_c) and tidal radius (r_t) of Sextans determined by different works. Using DECam, Roderick et al. (2016) suggested a tidal radius of 83.2 ± 7.1 , which is significantly smaller than the traditional value of $160' \pm 50'$ by Irwin & Hatzidimitriou (1995). Very recently, Cicuéndez et al. (2018), also using DECam, and Okamoto et al. (2017), with Suprime-Cam, challenged Roderick et al.'s (2016) findings by measuring a tidal radius of ~120'. If assuming Roderick et al.'s (2016) tidal radius, our survey covers virtually the full extension of Sextans. If the true r_t is closer to the value given by Okamoto et al. (2017) and Cicuéndez et al. (2018), our survey covers the galaxy completely along the semimajor axis, but it is incomplete along the semiminor axis.

Observations were taken during two observing runs in 2014 and 2017. Table 1 summarizes the DECam observations. The advantage of the short periods of DC stars is that the light curves can be fully sampled with a few hours of observations. Our strategy consisted of obtaining continuous observations of

Table 1Observing Log

| Field | α (J2000.0) | δ (J2000.0) | Date | N_g | N_r |
|-------|-------------|-------------|---------------|-------|-------|
| A | 10:09:12.0 | -02:21:01.4 | 2014 Mar 8-10 | 34 | 35 |
| В | 10:17:12.0 | -00:50:35.5 | 2014 Mar 8-10 | 38 | 38 |
| C | 10:13:03.0 | -01:31:53.0 | 2017 Apr 4 | 48 | 4 |

our field in two bands (g and r) for several consecutive hours each night. In 2014, we covered two fields at each side of the center of Sextans, placed along the semimajor axis of the galaxy (fields A and B; see Figure 1). In each of the first 2 nights of the 3 night run, we gave priority to a different field in order to obtain a set of continuous g, r exposures during \sim 6 hr and secure the observation of at least one full pulsational period of the DC stars. Nonetheless, a few observations of the other field were inserted through the night. The observing sequence consisted of 300 and 500 s in g and r, respectively. The third night, we alternated between the two fields continuously. In this observing run, we collected \sim 36 epochs per band per field. Although the cadence was designed for DC stars, having observations during 3 nights made the data set suitable for longer-period variables, such as RR Lyrae stars and anomalous Cepheids.

For the 2017 run, we had only 1 night available, so the observing strategy changed, and we prioritized the number of epochs over multiband observations. The goal for this run was to cover the central part of the galaxy (field C). We ran sequences of 10×300 s in g and 1×500 s in r consecutively for 5.5 hr, the time in which the galaxy was above an airmass of ~ 1.8 . In total, we obtained 48 and four observations in g and r, respectively. We note that CCD S30 was active during this run (contrary to the 2014 observing run). The seeing was stable and similar for both runs, with a median value of 1.126. The Moon was closer to Sextans during the 2017 observations. Consequently, the limiting g magnitude for the central field C is ~ 0.5 mag brighter than for fields A and B (0.25 mag brighter in the r band). Data are available through the NOAO Science archive.

2.1. Data Reduction and Photometry

Basic reduction of the data was done by the DECam Community Pipeline (Valdes et al. 2014), which includes a refinement of the WCS defined in the headers of the images. Point-spread function photometry was extracted from the images of each of the individual detectors in DECam using the DoPHOT software package (Schechter et al. 1993; Alonso-García et al. 2012). The instrumental positions of the sources reported by DoPHOT were transformed into ecliptic coordinates using WCSTools and the astrometric information provided in the headers of the reduced images. Extended objects flagged by DoPHOT were eliminated.

For each field, we chose reference catalogs in both filters based on the number of objects detected, seeing, and airmass. Photometry from the different epochs was first brought into the instrumental system defined by this reference catalog. Reference catalogs were first cleaned by eliminating all objects whose photometric error (σ_{star}) was larger than the photometric error of most of the stars of similar magnitude. This process

was accomplished by calculating a clipped mean and standard deviation (σ_m , rms) of the DoPHOT individual errors for all objects in bins of 0.25 mag. A curve of the maximum expected error ($\sigma_{\rm exp}$ (mag)) was defined as a spline function going through $\sigma_m + 5 \times {\rm rms}$. Objects that had $\sigma_{\rm star} > \sigma_{\rm exp}$ were eliminated from our working catalog. This process was particularly important to eliminate spurious detections within large galaxies, which were abundant in these fields.

In the next step, all catalogs were matched to the reference catalogs using STILTS⁷ (Taylor 2006) with a tolerance of 0."7. Only objects having a minimum of 12 observations in both g and r were kept. For field C, which was observed very few times in the r band, the minimum number was set to two in that band. Each catalog was normalized to the reference by calculating zero-point differences in each filter using all stars in common brighter than g, r = 20 mag, in each CCD. Typically, there were $\sim 80-100$ stars per CCD available for this calculation, and the resulting rms was usually < 0.02 mag. The zero points calculated this way were applied to all stars in each photometric catalog.

In Figure 2, we show the standard deviation of the magnitude distribution for each star as a function of mean magnitude for fields A and C. Field B, not shown, is very similar to A. Errors increase to 0.1 mag at g = 23.1 in fields A and B and g = 22.6 in field C. Variable stars are recognized in a plot like this because the standard deviation of the magnitude distribution is larger than the main locus observed in Figure 2, which correspond to stars that keep a constant magnitude within their photometric error. To characterize the loci of nonvariable stars, we binned the data in 0.25 mag bins and calculated the (σ -clipped) mean error, $\sigma(m)$, and standard deviation, std(m), in each bin centered on magnitude m. We consider stars as variable candidates if they are located significantly above the locus $(\sigma_{\text{star}} \geqslant \sigma \ (m) + 3 \times \text{std}(m))$ in both the g and r filters. In Figure 2, particularly for field C, the number of variable star candidates at $g \sim 20.5$ is very obvious. These stars correspond to the magnitude of the HB in Sextans, which is populated by numerous RR Lyrae stars.

Absolute calibration was made using Pan-STARRS1 (PS1) DR1⁸ photometry (Magnier et al. 2016). Each field was calibrated separately. We matched stars with PS1 with a tolerance of 1", selecting only stars with PS1 photometric errors <0.05 mag. Linear transformation equations (zero-point and color-term) between our instrumental magnitudes and the PS1 stars were calculated for each field using stars from all CCDs. We found no need to do this step on a CCD-by-CCD basis, since the results were similar for all CCDs, but errors are minimized by having a larger number of calibrating stars when using the full field. Between 2000 and 3500 stars were used for the calibration in each field. The rms of the fits is 0.02 mag in both g and r.

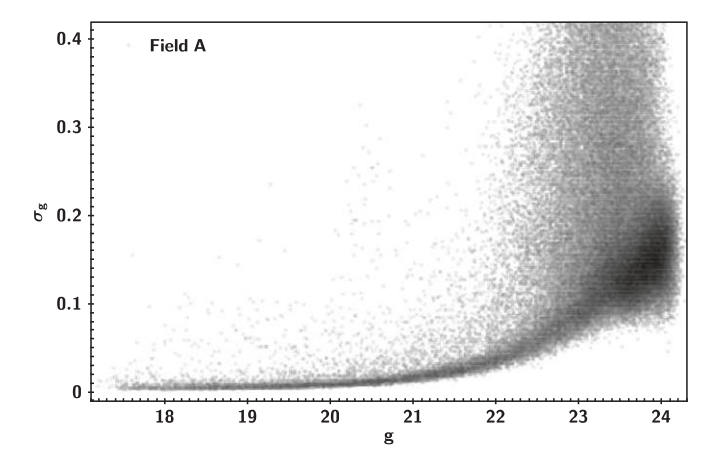
3. Variable Stars in the Instability Strip

Stars flagged as variable candidates, as described in the previous section, were searched for periodicity using a multiband implementation of the Lafler & Kinman (1965) algorithm, as described in Vivas & Mateo (2013). The method is a phase-dispersion minimization algorithm in which the correct period is the one that produces a smooth phased light

⁶ http://archive.noao.edu

http://www.star.bris.ac.uk/~mbt/stilts/

https://panstarrs.stsci.edu



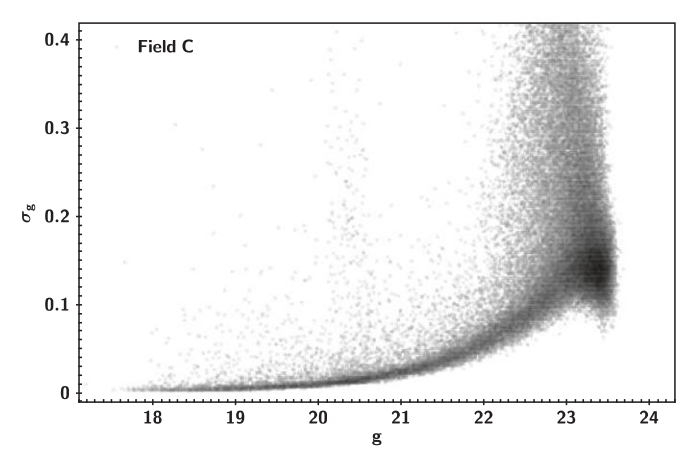


Figure 2. Standard deviation of the magnitude distribution in g for all stars in field A (top) and field C (bottom) as a function of mean magnitude.

curve. To optimize the search, we imposed a color constraint in order to include only variable star candidates in the instability strip. The color cut was loose enough, -0.5 < (g - r) < 0.62, to include a generous region around the instability strip but avoid searching through the large number of very red sources present in the color-magnitude diagram (CMD). To search for DC stars, we used trial periods ranging from 0.03 to 0.15 day, while for RR Lyrae stars and anomalous Cepheids, the range for searching was 0.15-0.9 day. The limited time baseline of the data does not allow us to search for periodicity beyond 1 day. All stars passing the cut $\Lambda > 2.0$ as defined by Lafler & Kinman (1965) were visually inspected. The parameter Λ quantifies the significance of the period selected as the best. In order to account for possible aliasing and spurious periods, the three best periods within the search range were inspected. Periodic variable stars were finally selected during this inspection, and classification was made based on the properties of the light curve (period and amplitudes) and their position in the CMD. Four stars had periods and light curves in agreement with them being either RR Lyrae or DC stars, but they were not in the corresponding place in the CMD for their type. Most likely, those stars are not Sextans members but just field stars in the foreground of the galaxy (but see discussion in Section 4).

Because there is overlap between fields, some variables were recognized independently in each field, which gave us confidence in our selection method. In those cases, we chose

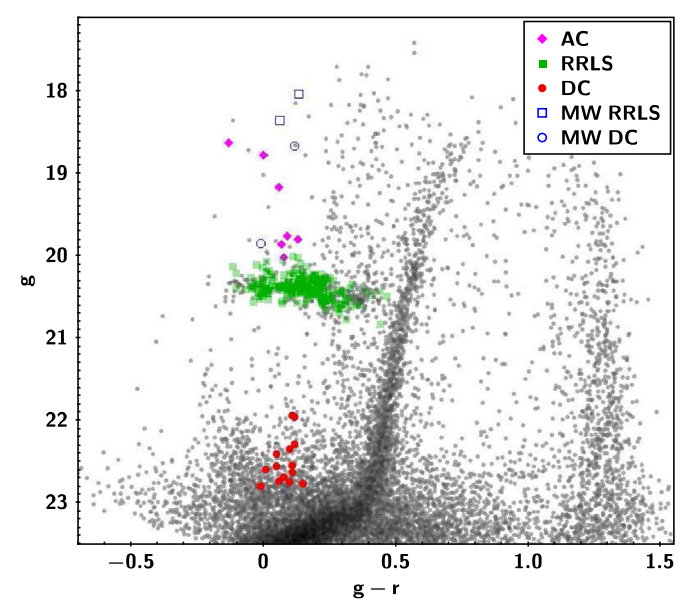


Figure 3. The CMD of Sextans. To better see the features of the galaxy, we only included stars within the core radius (26/8) of the galaxy. Pulsating variable stars detected in the full footprint of the survey are overplotted in the CMD with symbols as indicated in the legend.

the detection in fields A and B over the ones in C, since the latter does not have time series in r.

Figure 3 shows the CMD of Sextans with the variable stars identified. To better see the features of the Sextans galaxy, we limited the stars in the CMD to those inside an ellipse with a semimajor axis equal to the core radius of Sextans (we assumed the parameters derived by Roderick et al. 2016, including an ellipticity of 0.29 and position angle of 56°.7). The narrow red giant branch and subgiant branch of Sextans are clearly defined in this diagram. The HB contains numerous RR Lyrae stars. Figure 4 shows the spatial distribution of the different types of variables. In the next subsections, we discuss the main types of variables found in Sextans, from fainter to brighter.

3.1. DCs

The DCs were the main goal of this work. A total of 16 DCs were detected, although two of them are significantly brighter than the rest and above the HB. It is very likely that these two DC stars are actually field stars (see Figure 3), although it is still puzzling that they are both inside the tidal radius of Sextans (Figure 4). Figure 5 shows the light curves of the DC stars. For each star, we show the time series (top panels) and the phased light curves in both g and r (lower panels). The stars with only g data correspond to the ones detected in field C. The time span of the observations in field C was only 5.5 hr, but the top panels clearly show that it was possible to cover three to four pulsational cycles; hence, we could easily determine the periods. The position, light-curve properties (mean magnitudes, periods, and amplitudes), and distance to the center of Sextans (D_{Sex}) of these DC stars are recorded in Table 2. The last column in the table indicates if they belong to the Sextans galaxy or if they are field stars. The reported mean magnitudes in Table 2 are not plain averages but phase-weighted intensityaveraged magnitudes calculated following Saha & Hoessel (1990). This way to calculate the mean magnitudes avoids the biases toward minimum magnitudes (because as RR Lyrae

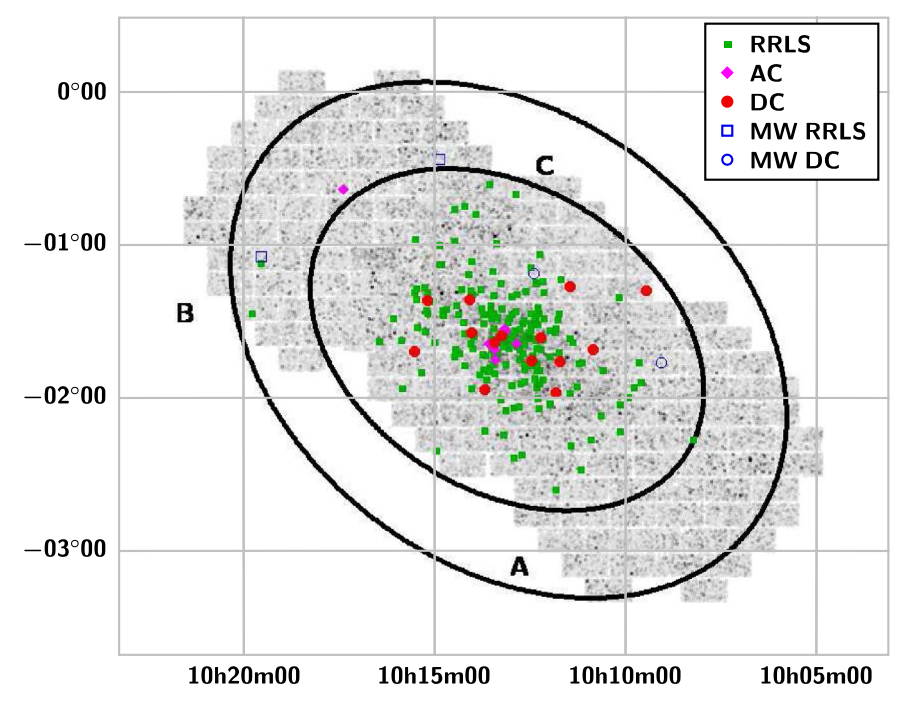


Figure 4. Map in equatorial coordinates of the main groups of variable stars found in this work. The inner and outer ellipses indicate a tidal radius of 83/2 (Roderick et al. 2016) and $r_t = 120'$ (Okamoto et al. 2017; Cicuéndez et al. 2018), respectively.

stars, some DC stars also spend most of their pulsation cycle time at minimum light) and those biases that may appear in unevenly sampled light curves. The reported r magnitudes for stars in field C are the straight average of the few (four) available measurements. Consequently, the colors for these stars may not be the true mean color.

The DC stars in Sextans occupy a narrow color range in the CMD, $\Delta(g - r) = 0.2 \,\text{mag}$, but display a large spread in magnitude, over \sim 0.8 mag in g between 21.9 and 22.7 mag. Periods range from 0.05 to 0.09 day, with a mean of 0.0646 day. Most of the light curves shown in Figure 5 look similar to the asymmetrical type ab RR Lyrae stars, although a few seem more sinusoidal. However, it is well known that the pulsation mode cannot be recognized in DC stars based on either the light-curve shape or a period-amplitude diagram (e.g., Vivas & Mateo 2013). Thus, the asymmetrical light curves in this case do not necessarily mean that those DC stars are pulsating in the fundamental mode. The amplitudes of variation displayed by the DC stars is large, ranging from $\Delta_g = 0.58$ to 1.14 mag, with a mean of 0.87 mag. However, it is possible that, given our photometric errors (~0.1 mag at g = 22.6 in the central field C), we are missing loweramplitude variable stars. In Figure 6, we show the g-band amplitude of the DC stars as a function of mean g magnitude. Based in our past experience in Carina (Vivas & Mateo 2013), it should be possible to detect variables with amplitudes of >0.2 mag if the photometric errors are ≤ 0.05 mag. When the errors increase to ~ 0.09 mag, the minimum amplitude that can be detected is ~ 0.4 mag. Accordingly, the dotted and dashed lines in Figure 6 show the minimum amplitude that can be detected in our survey. Although we may indeed be missing low-amplitude variables, particularly in the central field C, it is nonetheless surprising that the lowest amplitude of our DC stars is \sim 0.6 mag, well above our detection limit. Galaxies like Carina or the LMC have plenty of stars with amplitudes in the range 0.2–0.6 mag (Garg et al. 2010; Vivas & Mateo 2013).

A comparison of the properties of DC stars in Sextans with other extragalactic systems will be discussed later in this paper.

3.2. RR Lyrae Stars

The RR Lyrae stars are by far the most numerous group of variable stars in Sextans. We detected 199 RR Lyrae variables, 65 of which are new discoveries and two of which are likely foreground stars. The RR Lyrae stars have been detected in Sextans before by Mateo et al. (1995) and Amigo (2012), although their studies only cover the central part of the galaxy (Figure 7). Lee et al. (2003) also previously selected RR Lyrae star candidates in an area similar to that of Amigo (2012) based on variability between two different epochs, but clearly, characterization of the light curves was not possible. More recently, two large-scale RR Lyrae star surveys partially covered the Sextans galaxy. The La Silla-QUEST survey (LSQ; Zinn et al. 2014) covers the full extent of Sextans, but the faint limit of that survey is just at the magnitude of the HB in Sextans. Consequently, only a handful of stars were detected. Interestingly, there is one star from that survey just outside the Roderick et al. (2016) tidal radius of Sextans (although it is inside if considering the tidal radius by either Irwin & Hatzidimitriou 1995 or Cicuéndez et al. 2018). On the other hand, the High Cadence Transient Survey (Förster et al. 2016; Medina et al. 2018) studied three DECam fields near (but not centered on) Sextans and measured 66 RR Lyrae stars, many of which were new discoveries, since their fields were located in the outskirts of Sextans. Joining all of these works together, Sextans has 227 RR Lyrae stars (Figure 7). We missed several of the known RR Lyrae stars due mostly to the gaps between the CCDs, since our observations were not dithered. Coordinates, light-curve properties, and identification in other surveys of all RR Lyrae stars detected in this work are provided in Table 3, and the light curves are shown in Figure 8.

For the stars in fields A and B, which have good sampling over the full light curve in both the g and r filters, we fitted

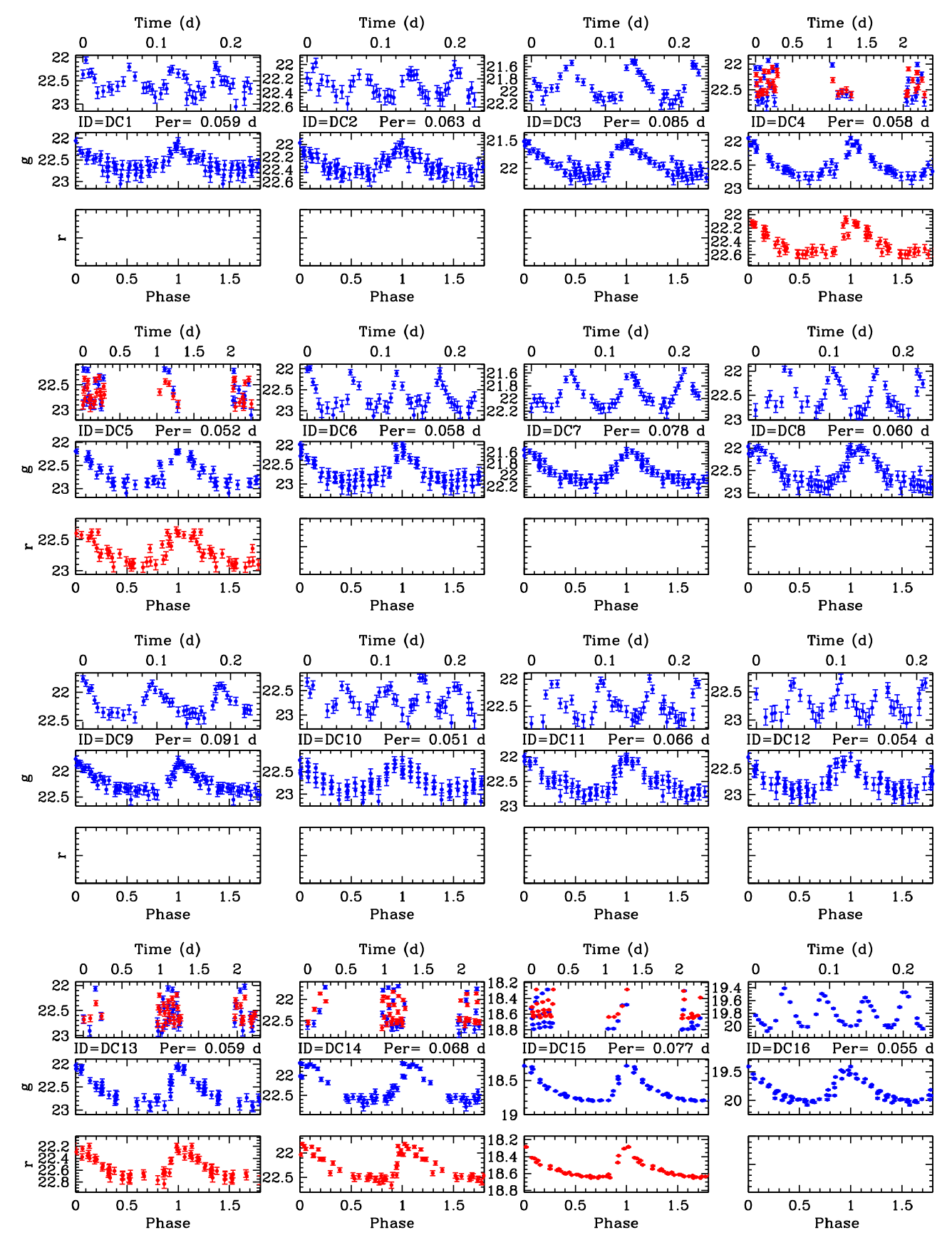


Figure 5. Light curves of the 16 DC stars found in Sextans. Magnitudes in g and r are shown with blue and red, respectively. The top panel for each star is the time series in days from the time of the first observation. The two lower panels show the phased light curve. Stars DC15 and DC16 are likely field stars.

Table 2 DC Stars

| ID | α (J2000.0) (deg) | δ (J2000.0) (deg) | N_g | N_r | $\langle g \rangle$ (mag) | $\langle r \rangle$ (mag) | Period (day) | Δ_g (mag) | Δ_r (mag) | D _{Sex} (arcmin) | Comment |
|------|----------------------|----------------------|-------|-------|---------------------------|---------------------------|-----------------|------------------|------------------|---------------------------|---------|
| DC1 | 152.37167 | -1.29472 | 47 | 4 | 22.59 | 22.58 | 0.0591 | 0.99 | | 56.5 | Sex |
| DC2 | 152.71577 | -1.68032 | 47 | 4 | 22.34 | 22.24 | 0.0631 | 0.58 | | 33.1 | Sex |
| DC3 | 152.86590 | -1.27122 | 46 | 4 | 21.93 | 21.82 | 0.0853 | 0.70 | | 30.9 | Sex |
| DC4 | 152.92910 | -1.75998 | 34 | 35 | 22.54 | 22.43 | 0.0576 | 0.89 | 0.54 | 22.2 | Sex |
| DC5 | 152.96042 | -1.96451 | 32 | 35 | 22.74 | 22.68 | 0.0521 | 0.91 | 0.60 | 28.4 | Sex |
| DC6 | 153.05480 | -1.60169 | 48 | 4 | 22.76 | 22.61 | 0.0583 | 1.14 | | 12.5 | Sex |
| DC7 | 153.11685 | -1.75687 | 48 | 4 | 21.96 | 21.84 | 0.0783 | 0.68 | | 12.8 | Sex |
| DC8 | 153.31278 | -1.59130 | 43 | 4 | 22.62 | 22.51 | 0.0604 | 0.95 | | 3.1 | Sex |
| DC9 | 153.35546 | -1.63900 | 46 | 4 | 22.28 | 22.16 | 0.0914 | 0.79 | | 6.0 | Sex |
| DC10 | 153.42480 | -1.94532 | 45 | 4 | 22.79 | 22.80 | 0.0509 | 0.94 | | 22.9 | Sex |
| DC11 | 153.50747 | -1.56894 | 45 | 4 | 22.56 | 22.51 | 0.0662 | 0.83 | | 14.8 | Sex |
| DC12 | 153.52053 | -1.35718 | 41 | 4 | 22.75 | 22.65 | 0.0543 | 0.78 | | 21.3 | Sex |
| DC13 | 153.79662 | -1.36580 | 36 | 38 | 22.68 | 22.60 | 0.0588 | 0.91 | 0.64 | 35.0 | Sex |
| DC14 | 153.87762 | -1.69308 | 36 | 38 | 22.41 | 22.36 | 0.0679 | 1.10 | 0.84 | 37.3 | Sex |
| DC15 | 152.26788 | -1.77082 | 34 | 35 | 18.67 | 18.55 | 0.0769 | 0.51 | 0.37 | 60.5 | Field |
| DC16 | 153.10447 | -1.18371 | 48 | 4 | 19.85 | 19.86 | 0.0551 | 0.67 | ••• | 26.7 | Field |

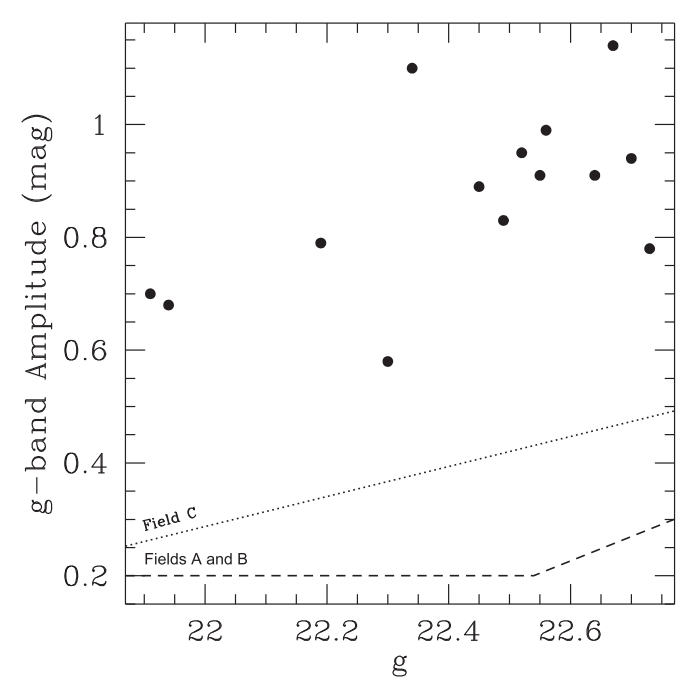


Figure 6. Amplitude of the DC stars as a function of mean magnitude. The dashed and dotted lines indicate the expected minimum amplitude that can be measured in fields A (similar to field B) and C, respectively.

templates to the data in order to better characterize the light curve. We used the library of templates set up by Sesar et al. (2010) based on SDSS Stripe 82 RR Lyrae stars. We first fitted the template in the band containing the larger number of epochs. The fitting was done by χ^2 minimization, covering a range of periods, initial phase, amplitude, and magnitude at maximum light around the observed values and the period given by the Lafler & Kinman (1965) method. We used the resulting period and initial phase as constants to fit the template in the other band. An example of a star for which we applied this procedure is RR1 (see Figure 8).

On the other hand, the time baseline of the observations in field C (the central field) was not adequate for RR Lyrae stars,

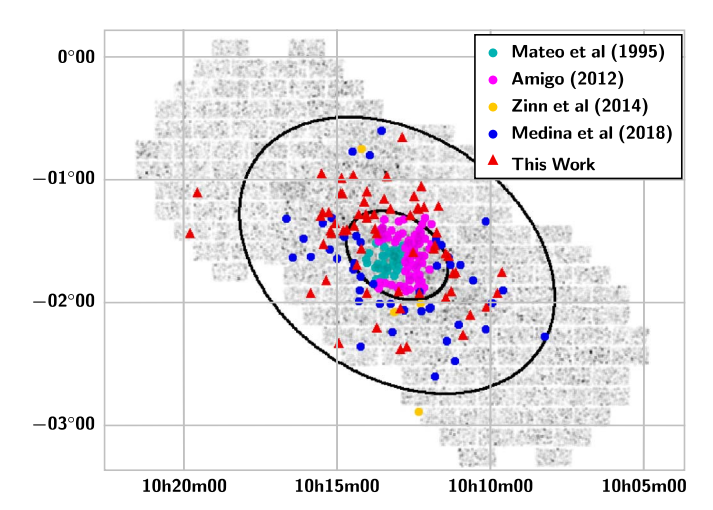


Figure 7. Distribution in the sky of RR Lyrae stars in the Sextans dSph. The color code indicates the first work that identified each RR Lyrae star. The two ellipses correspond to the core radius ($r_c = 26/8$) and tidal radius ($r_r = 83/2$) as determined by Roderick et al. (2016). Although most of the RR Lyrae stars are concentrated toward the center of the galaxy, there are several in the outskirts. In particular, there are three RR Lyrae stars outside the tidal radius (as determined by Roderick et al. 2016), one from the LSQ (Zinn et al. 2014) and two from this work.

since it only covered a fraction of a single pulsation cycle. The search for RR Lyrae stars was done in a different way in this field. In 5.5 hr of continuous observations, we covered \sim 35% of the pulsation cycle of type ab stars and \sim 75% of the cycle for RRc. These are long enough ranges for recognizing RR Lyrae stars in a simple look at the Julian date versus magnitude plot. Thus, we looked for continuous variation in the time series of the variable star candidates in the selected color range. No attempt at period finding was performed. However, since the central field of Sextans has been explored before for RR Lyrae stars, we used the known periods of stars in common with other studies and fitted light-curve templates to the time series. During the fitting process, we allowed generous variations in amplitude (around the literature value), initial phase, and magnitude at maximum light, but the period was kept constant. Star RR8 (Figure 8) is an example of one of the stars in which this procedure was used.

Table 3
RR Lyrae Stars

| ID | α (J2000.0) (deg) | δ (J2000.0) (deg) | Type | Period (day) | MJD ₀ (days) | N_g | Δ_g (mag) | $\langle g \rangle$ (mag) | g _{max} (mag) | $\sigma_{\rm fit} (g)$ (mag) | Template (g) |
|----------------------|----------------------|---------------------------|------|------------------------|----------------------------|-------|------------------|---------------------------|------------------------|------------------------------|--------------|
| RR1 | 152.06381 | -2.27372 | ab | 0.6948 | 56,726.30554 | 32 | 0.94 | 20.29 | 19.74 | 0.02 | 111g.dat |
| RR2 | 152.40204 | -1.89860 | c | 0.3457 | 56,724.17884 | 34 | 0.61 | 20.36 | 20.08 | 0.07 | 0g.dat |
| RR3 | 152.41282 | -1.76577 | ab | 0.7487 | 56,726.09288 | 34 | 0.56 | 20.30 | 19.98 | 0.01 | 101g.dat |
| RR4 | 152.44702 | -1.93215 | c | 0.2987 | 56,725.25898 | 34 | 0.23 | 20.30 | 20.19 | 0.01 | 0g.dat |
| RR5 | 152.48994 | -1.99834 | ab | 0.6553 | 56,725.10121 | 33 | 0.86 | 20.38 | 19.90 | 0.04 | 101g.dat |
| N _r (mag) | Δ_r (mag) | $\langle r \rangle$ (mag) | | r _{max} (mag) | $\sigma_{ m fit} (r)$ | Те | mplate (r) | | Other Nan | nes | Comment |
| 35 | 0.67 | 20.12 | | 19.75 | 0.01 | 1 | 109r.dat | Н | iTS100815-0 |)21625 | Sextans |
| 34 | 0.46 | 20.31 | | 20.09 | 0.06 | | 1r.dat | Н | iTS100936-0 |)15356 | Sextans |
| 35 | 0.42 | 20.08 | | 19.86 | 0.01 | 1 | 04r.dat | | | | Sextans |
| 34 | 0.16 | 20.28 | | 20.21 | 0.01 | | Or.dat | | | | Sextans |
| 33 | 0.74 | 20.19 | | 19.79 | 0.03 | 1 | 09r.dat | Н | iTS100958-0 |)15954 | Sextans |

(This table is available in its entirety in machine-readable form.)

The mean magnitude reported in Table 3 was obtained by integrating the template in intensity units and transforming the result back to magnitude. On average, the rms of the template fits is ~ 0.03 mag. The mean r values for stars in field C are straight averages of the available observations.

There were, however, several RR Lyrae star candidates (29 stars) in field C that were not known before, and without knowledge of the period, we cannot characterize the light curve. Their location in the CMD and the smooth variations observed in the 5.5 hr period secure their classification as RR Lyrae stars. We report them too in Table 3 and Figure 8 (see, for example, star RR11). The mean magnitudes for the stars in this group are simple averages of the available observations in each band.

Among the Sextans RR Lyrae stars, we were able to classify 125 as RRab, 41 as RRc, and two as RRd. As mentioned before, 29 stars were not classified due to insufficient time coverage. The ab and c groups have mean periods of 0.616 and 0.369 day, respectively. The mean period of the RRab stars in Sextans classifies this galaxy in the class Oosterhoff-intermediate, in agreement with previous works (Mateo et al. 1995). A full discussion of the properties of RR Lyrae stars in Sextans will be deferred to a future paper (C. Martínez-Vázquez et al. 2018, in preparation).

Two RR Lyrae stars (RR33 and RR47) have been classified as double-mode pulsators, or RRd. The star RR33 was previously known (C9 in Amigo 2012), and our classification is in agreement with the one given by Amigo (2012). No template fitting was possible in those cases. Table 3 reports the first overtone periods. The fundamental periods are likely 0.580 and 0.554 day for RR33 and RR47, respectively. Seven additional stars (RR32, RR39, RR49, RR112, RR128, RR133, and RR144) have also been reported by Amigo (2012) to be double-mode pulsators. However, our limited time coverage data on these stars, all of them in field C, show them as c-type pulsators, which is the classification we have given in Table 3.

Another two RR Lyrae stars (RR198 and RR199) have mean magnitudes significantly brighter than the HB of Sextans (see Figure 3). They are also located well outside the Roderick et al. (2016) tidal radius of the galaxy (Figure 7). Thus, these two stars are likely field stars along the same line of sight of

Sextans, although we discuss the possibility that they are actually anomalous Cepheids of Sextans in Section 4.

3.3. Anomalous Cepheids

Anomalous Cepheids are a common type of variable star found in dSph galaxies (Clementini 2014). Their existence in these galaxies is usually interpreted as due to the presence of an intermediate-age population, since these are metal-poor, $1.3-2.0\,M_{\odot}$ stars in the core helium-burning phase (Fiorentino & Monelli 2012). However, an additional mechanism to bring stars to this part of the instability strip is through mass transfer in an old binary system (Gautschy & Saio 2017). Mateo et al. (1995) identified six anomalous Cepheids in Sextans, and Amigo (2012) increased that number to eight. Here we have recovered six of them (the other two were in gaps between the DECam CCDs), and we found an additional star, AC7, in Table 4. Light curves are shown in Figure 9. Similar to what we did for the DC stars (Section 3.1), the mean magnitudes in Table 4 are phase-weighted intensity-averaged values, except for the r band in field C, which is just straight averages. Because the light curves of these stars are not completely sampled, the reported mean magnitudes may not be accurate. The six known anomalous Cepheids were all located in field C, and consequently, our data do not constrain the light-curve properties well. The periods listed in Table 4 for these stars come from Amigo (2012). The amplitudes in the table come from our data, but they are not well constrained, since we do not observe a full cycle for these stars. This is particularly true for AC3 and AC4, for which we cover only part of the light curve at minimum light. Our new discovery, AC7, was located in field B, the period and amplitudes in both g and r are well constrained by our data, and its properties and location in the CMD agree well with the classification as an anomalous Cepheid.

Surprisingly, however, AC7 is not located toward the center of the galaxy like the rest of the anomalous Cepheid stars in Sextans. Instead, it is located just outside the tidal radius of the galaxy (as measured by Roderick et al. 2016). We considered the possibility that this star is actually a foreground RR Lyrae star within our footprint. The amplitude and shape of the light curve seem to indicate that this may be an RRab star. The period (0.4104 day) is somewhat short for an RRab star but not

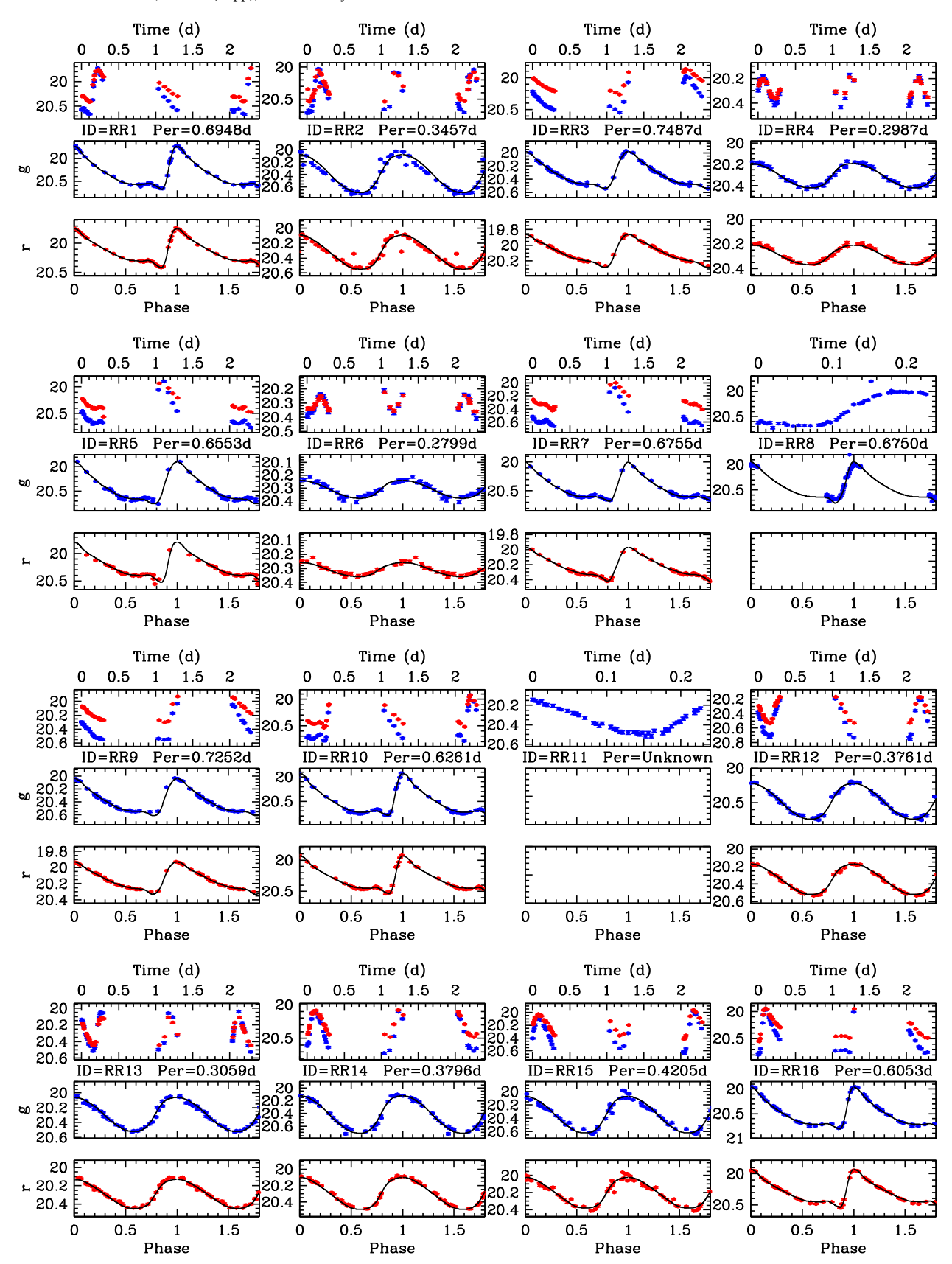


Figure 8. Light curves of the RR Lyrae stars detected in this work. The top panel for each star is the time series in days from the time of the first observation. This encompass three consecutive nights for some stars (those in fields A and B) and only 5.5 hr (or \sim 0.23 day) for stars in field C. For the latter group, only g time series are available, and phase light curves (two lower panels for each star) are shown only for stars with previously known periods (see text).

(The complete figure set (13 images) is available.)

Table 4
Anomalous Cepheids

| ID | α (J2000.0) (deg) | δ (J2000.0) (deg) | N_g | N_r | $\langle g \rangle$ (mag) | $\langle r angle$ (mag) | Period (day) | $\Delta_g \pmod{mag}$ | Δ_r (mag) | Other Name |
|-----|----------------------|----------------------|-------|-------|---------------------------|--------------------------|-----------------|-----------------------|------------------|------------|
| AC1 | 153.21128 | -1.64243 | 46 | 4 | 18.78 | 18.78 | 0.9198 | 0.73 | ••• | V6 |
| AC2 | 153.28425 | -1.56633 | 46 | 4 | 20.02 | 19.94 | 0.4160 | 0.90 | | V9 |
| AC3 | 153.29410 | -1.54672 | 46 | 4 | 18.64 | 18.77 | 0.5207 | 0.08 | | C82 |
| AC4 | 153.35253 | -1.74856 | 46 | 4 | 19.76 | 19.67 | 0.4046 | 0.16 | | C89 |
| AC5 | 153.35785 | -1.68251 | 46 | 4 | 19.86 | 19.79 | 0.5069 | 0.48 | | V34 |
| AC6 | 153.39361 | -1.64499 | 46 | 4 | 19.17 | 19.11 | 0.8609 | 0.83 | | V5 |
| AC7 | 154.34301 | -0.63833 | 38 | 38 | 19.81 | 19.68 | 0.4104 | 0.85 | 0.62 | ••• |

completely impossible (Samus et al. 2017). A mean g magnitude of 19.72 will locate AC7 at ~53 kpc from the Sun (after correcting by interstellar extinction) if it is an RR Lyrae star. Stars at such large distances in the Galactic halo are rare. We integrated the number density radial profile of RR Lyrae stars derived by Medina et al. (2018) using a large sample of distant stars and found that we should expect 0.25 RR Lyrae star in the range of distances 50–60 kpc in the 7 deg² area covered by our survey. Thus, it would not be completely impossible that this is indeed a foreground RR Lyrae star. However, short-period abtype RR Lyrae stars are usually associated with high metallicity (for example, Maintz & de Boer 2005; Skarka 2014), which would be unusual given its large distance from the Sun and location above the galactic plane ($b \sim 40^{\circ}$). We discuss more on the spatial distribution of the variables in Sextans and the possibility of extratidal variable stars in the next section.

4. Spatial Distribution of the Variable Stars in Sextans

Figure 4 shows that the distribution in the sky of the bulk of the variables detected in this work is concentrated toward the center of the galaxy in a rather "boxy" shape, following the distribution of the Sextans stellar population (see stellar density maps in Figures 7 and 13 in Roderick et al. 2016). More than half of the variable stars (58%) are indeed contained within the 26.8 core radius of Sextans. This central concentration distribution holds for the three types of pulsating variables that we have found in this work. This is not a selection effect, since we actually have better temporal coverage and deeper observations in the two outermost fields of our survey.

There are three variable stars, two RR Lyrae (RR196 and RR197) and one anomalous Cepheid (AC7), that lie outside the 83'.2 tidal radius of Sextans. As discussed before (Section 2), the above tidal radius (Roderick et al. 2016) is significantly smaller than the ones given in other works in the literature. In the discovery paper, Irwin et al. (1990) measured a tidal radius of 90', which was revised later by Irwin & Hatzidimitriou (1995) to $r_t = 160'$. Recently, both Okamoto et al. (2017) and Cicuéndez et al. (2018) also suggested a large tidal radius, 120'. Thus, the possibility of being extratidal stars only holds if the tidal radius is indeed as short as that suggested by Roderick et al. (2016).

The three stars presumed to be extratidal are located toward the NE side of Sextans. This, however, may be a selection effect, since we covered the galaxy only along the semimajor axis; thus, we cannot say if there is debris along the semiminor axis. Evidence for extratidal material in this galaxy is hard to prove because of its large low surface brightness and field contamination, especially at large distances from its center. Variable stars are then a particularly useful tracer of possible

extratidal material, and the stars we have found may indicate that the galaxy is disrupting. In order to further test this scenario, we studied the proper motions of the variable stars in Sextans in Gaia DR2 (Gaia Collaboration et al. 2016, 2018a). First, we isolated Sextans stars (variable or not) by selecting from all DR2 objects within the core radius of Sextans (black plus signs in the top left panel of Figure 10) those in the red giant branch and HB of Sextans that have errors in the proper motion <2 mas yr⁻¹ (red circles). The proper motions of that sample of \sim 1000 Sextans stars are shown in the top right panel of Figure 10. The vertical and horizontal dashed lines indicate the mean proper motion, $(\mu_{\alpha}^{*}, \mu_{\delta}) = (-0.496, 0.077) \text{ mas yr}^{-1}$, as derived by Gaia Collaboration et al. (2018b). Our selection of Sextans stars is clumped together in proper-motion space around those values. For comparison, we show in the bottom right panel the proper-motion distribution of non-Sextans stars in the field. To select this population, we used our full catalog but did not include either stars inside the locus of the HB and red giant branch or stars with proper-motion errors >1.0 mas yr⁻¹. Although some contamination by Sextans stars seems to still be present in this figure, it is clear that the foreground population in the field concentrates in the fourth quadrant of this diagram (negative proper motions in both coordinates), which mostly separates from the bulk of the Sextans population.

We then matched our list of variable stars with Gaia DR2. Out of our list of 222 variable stars (of all types), a total of 117 have measured proper motions in the Gaia DR2 data set. As expected, none of the DC stars in our sample had a counterpart in DR2, since these stars are beyond the Gaia limiting magnitude. All of the anomalous Cepheids but AC1 had a proper-motion measurement. In Figure 10 (bottom left), we show the proper motion of the RR Lyrae stars and anomalous Cepheids found in Gaia. As expected, they nicely clump together around the Sextans proper motions. Our three possible extratidal stars are labeled and shown with large symbols in Figure 10 (bottom left). All three of them have proper motions in agreement with being Sextans members and may be extratidal material. In particular, AC7, which is a bright star (g = 19.72), has relatively small error bars in its proper motion $(\sigma \mu_{\alpha} = 0.90 \text{ mas yr}^{-1}, \ \sigma \mu_{\delta} = 0.83 \text{ mas yr}^{-1}), \text{ and it is within}$ 1σ of the mean proper motion of Sextans.

In the left bottom panel of Figure 10, we also highlight the case of RR199, which is one of the two RR Lyrae stars that we classified as a field variable. The other star is RR198, which unfortunately has no counterpart in *Gaia* DR2. These two stars were also located outside the tidal radius of Sextans (blue squares in Figure 4) but were marked as RR Lyrae stars because of their location, as well as the fact that they were quite

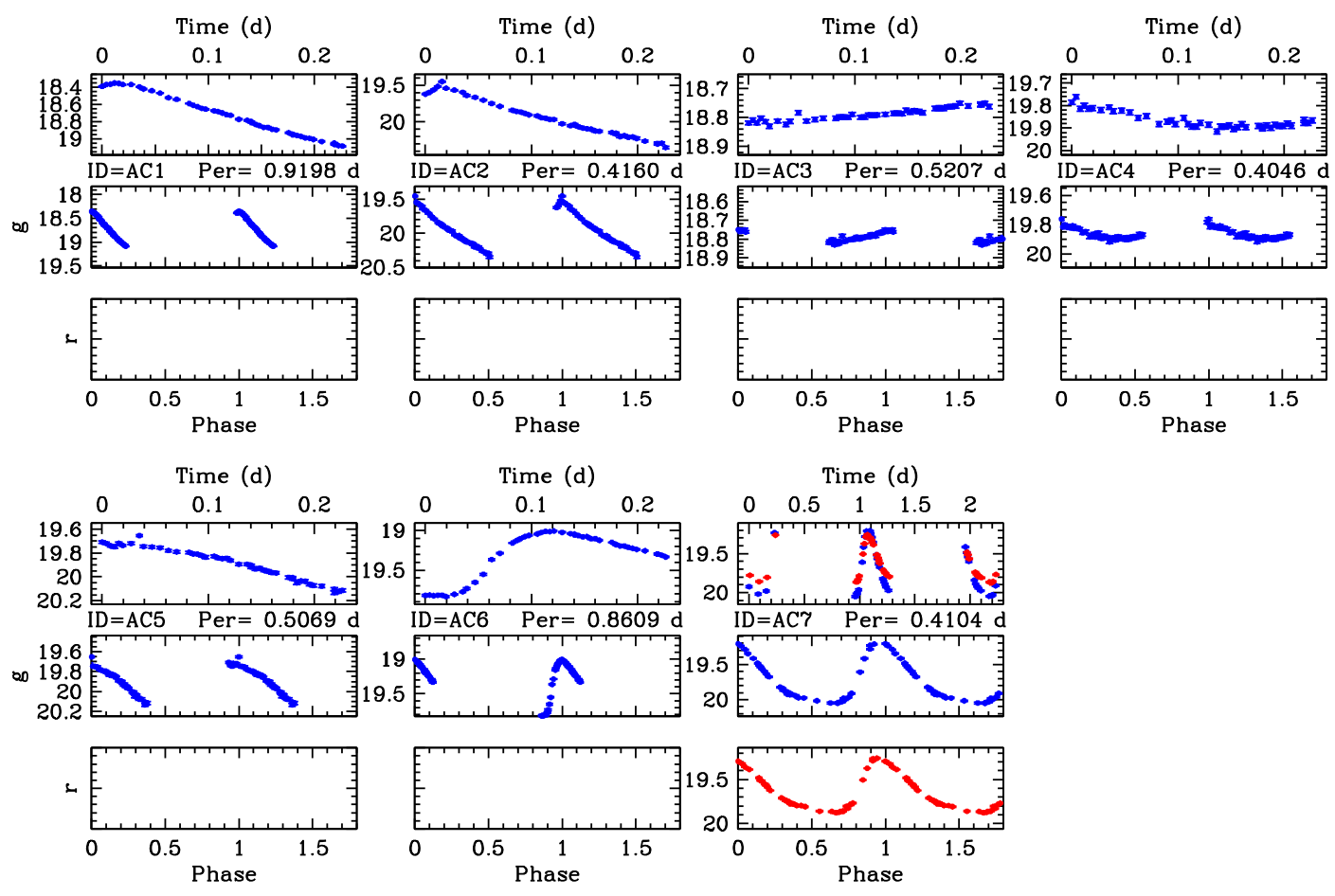


Figure 9. Light curves of the seven anomalous Cepheid stars detected in this work. The top panel for each star is the time series in days from the time of the first observation. The two lower panels show the phased light curves in g and r. Periods for AC1–AC6 were taken from Mateo et al. (1995) and Amigo (2012). Only for AC7 (a new discovery) were we able to determine the period from our own data.

bright, brighter than the rest of the anomalous Cepheid stars. The period range of anomalous Cepheids overlaps with that of the RR Lyrae stars, and there is no easy way to distinguish one from the other if the distance is not known (Catelan & Smith 2015). If they are RR Lyrae stars, their magnitudes locate these stars at 28 and 29 kpc from the Sun. We expect one (±1) halo RR Lyrae star in our footprint with distances between 25 and 35 kpc, according to the number density profile of the halo by Medina et al. (2018). The proper motion of RR199, however, shows compatibility with being a Sextans member. This opens up the possibility that RR199 is not really a field RR Lyrae star but an extratidal anomalous Cepheid in Sextans, similar in that respect to AC7. The star RR199 is separated by 2 mag from the mean of the RR Lyrae stars in the Sextans HB (open blue squares in Figure 3). This large Δ mag between the anomalous Cepheid and the HB has also been observed in other systems—for example, in Carina (Coppola et al. 2015) and Leo I (Stetson et al. 2014)—although the latter may contain a mix of anomalous Cepheids and short-period classical Cepheids. For RR198, there are no proper motions available, but it has similar properties to RR199 in the CMD. Both stars are also located toward the NE side of Sextans, similar to the other extratidal variable stars mentioned above. Radial velocities are needed to settle if they are indeed Milky

Way foreground RR Lyrae stars or Sextans anomalous Cepheid variables.

5. The Distance to Sextans from Its RR Lyrae Stars

Before introducing the behavior of the Sextans DC stars in a PL diagram and comparing with other works, we will anchor the distance of Sextans to its RR Lyrae stars. The mean magnitudes for the variable stars were corrected by interstellar extinction using the following equations with coefficients taken from Schlafly & Finkbeiner (2011) for PS1 magnitudes (their Table 6), in combination with the color excesses E(B-V) from the dust maps of Schlegel et al. (1998): $A_g=3.172E(B-V)$ and $A_r=2.271E(B-V)$. A map of the color excess in the Sextans region is shown in Figure 11. Although this is a high-latitude region, the area covered by Sextans is large enough that significant differences in reddening are observed throughout the galaxy.

We used the following g and r period–luminosity–metallicity (PLZ) relationship for RRab stars in the PS1 magnitude system, taken from Sesar et al. (2017):

$$M_g = -1.7 \log(P/P_{\text{ref}}) + 0.08([\text{Fe/H}] - [\text{Fe/H}]_{\text{ref}}) + 0.69,$$
(1)

$$M_r = -1.6 \log(P/P_{\text{ref}}) + 0.09([\text{Fe/H}] - [\text{Fe/H}]_{\text{ref}}) + 0.51,$$
(2)

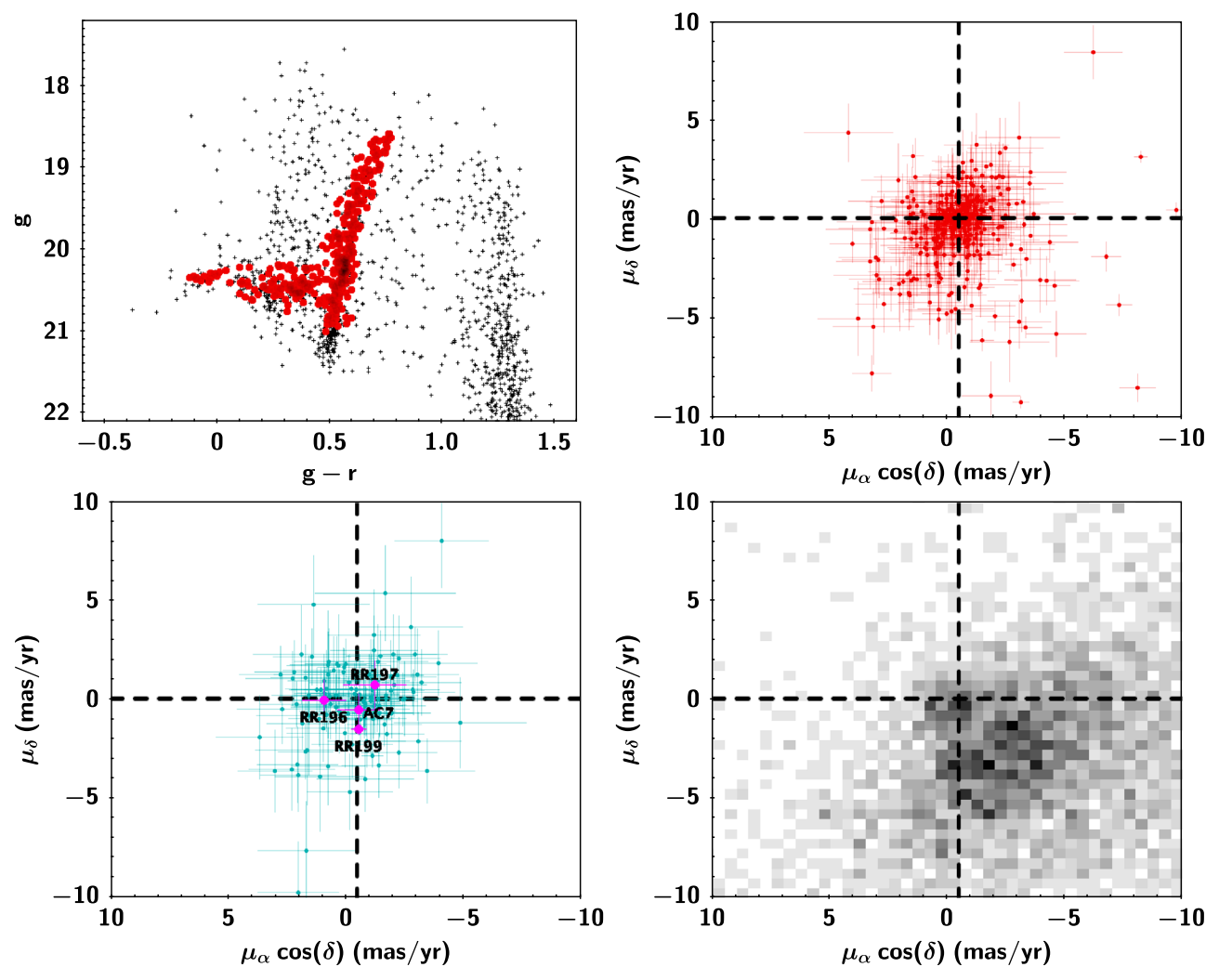


Figure 10. (Top left) The CMD of the *Gaia* DR2 stars that matched with our catalog in the region within the core radius of Sextans. We selected from there only stars with an error in the proper motion <2 mas yr^{-1} and in either the red giant branch or HB of Sextans (red circles). (Top right) Proper-motion distribution of Sextans stars as selected in the previous panel. (Bottom left) Proper motion of 117 variable stars in our survey that matched *Gaia* DR2. The extratidal candidates have been labeled. (Bottom right) Proper motion of foreground population. Only stars with proper-motion errors <1.0 mas yr^{-1} were included in this panel.

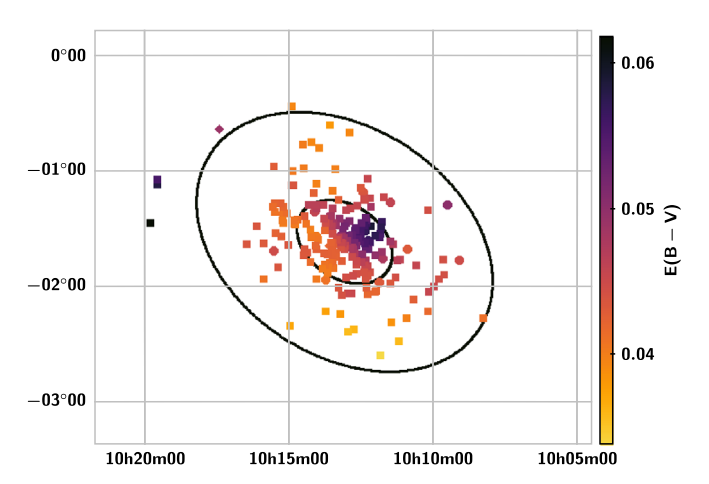


Figure 11. Map (R.A. vs. decl.) of the color excess E(B-V) from Schlegel et al. (1998) toward each variable star found in this work (squares, RR Lyrae stars; circles, DCs; diamonds, anomalous Cepheids). The two ellipses correspond to r_c and r_t as determined by Roderick et al. (2016).

where $P_{\text{ref}} = 0.6 \,\text{day}$ and $[\text{Fe/H}]_{\text{ref}} = -1.5 \,\text{dex}$. The rms values of these relationships are 0.07 and 0.06 mag in g and r, respectively. We applied these PLZ relationships assuming a mean metallicity for Sextans of $[Fe/H] = -1.93 \, dex$ (Kirby et al. 2011). The dependence with period of these relationships is in excellent agreement with our data (Figure 12). To calculate the mean distance modulus to Sextans from the RRab stars, we used only the 42 stars for which we had complete coverage of their light curves (the ones in fields A and B). They are shown as circles in Figure 12. Although we fitted templates to the g light curves of stars in field C reasonably well, for many stars, the coverage of the observations is not enough to cover the full amplitude of the variation, and there is uncertainty in the final amplitudes. This is particularly true for stars that do not have observations near maximum light (see, for example, RR29 in Figure 8). Consequently, the mean magnitude of the RR Lyrae stars in field C, which is calculated by integrating the fitted template, may not be accurate.

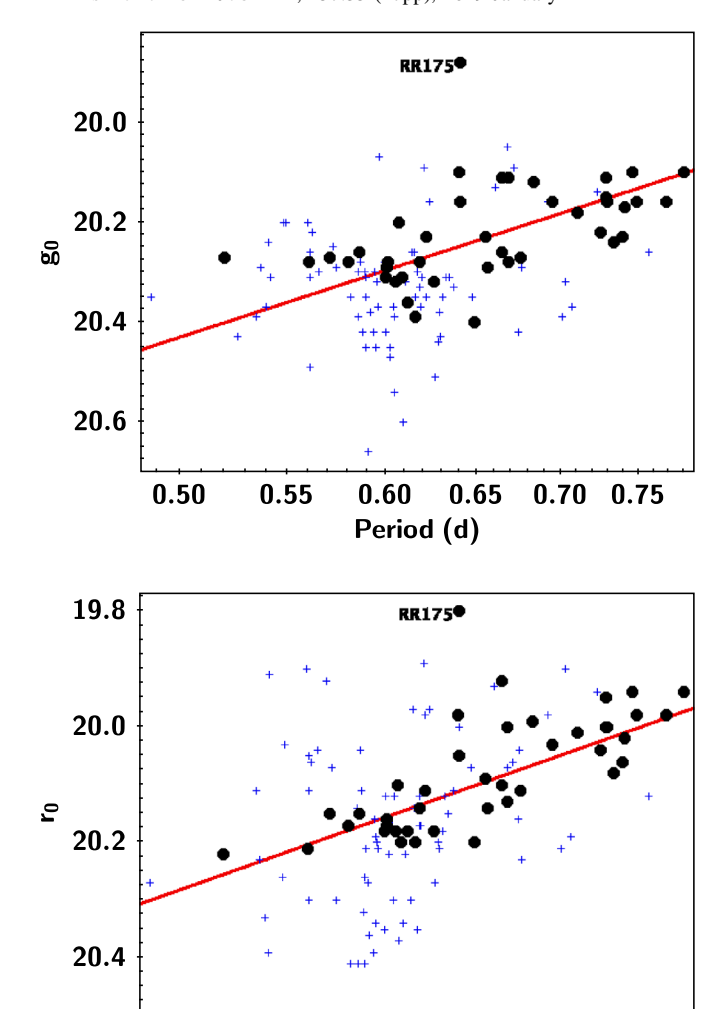


Figure 12. Extinction-corrected magnitudes g_0 (top) and r_0 (bottom) of the Sextans RR Lyrae stars vs. period. The RR Lyrae stars in fields A and B that have complete light curves available are shown with circles. Stars in field C, which have only partially observed light curves, are shown with plus signs. The red line is not a fit to our data but a representation of Equations (1) and (2) with [Fe/H] = -1.93 and shifted by a distance modulus of 19.64 and 19.68 in g and r, respectively. The star RR175 may be an evolved RR Lyrae star or an anomalous Cepheid.

0.60

Period (d)

0.65

0.50

0.55

0.70 0.75

Figure 12 shows that the stars in field C (plus signs) also follow the PLZ of the well-observed stars, but understandably, they display more dispersion. In the *r* band, the dispersion is even larger, since there are only four observations per star in this band, and the mean magnitudes are straight averages of those. Among the sample of well-observed RR Lyrae stars, one star, RR175, is significantly brighter than the rest of the stars in both bands. It is possible that RR175 is either an evolved RR Lyrae star or an anomalous Cepheid.

The mean distance modulus and error of the mean from the g light curves of 41 RRab stars (excluding RR175) are 19.64 \pm 0.01 mag, while in the r band, we obtained 19.677 \pm 0.008. These are equivalent to 84.7 and 86.2 kpc from the Sun, which is in excellent agreement with previous estimates, for example, 84.2 kpc from Medina et al. (2018) and 86 kpc from Mateo et al. (1995) and Lee et al. (2009). Because most of the DC

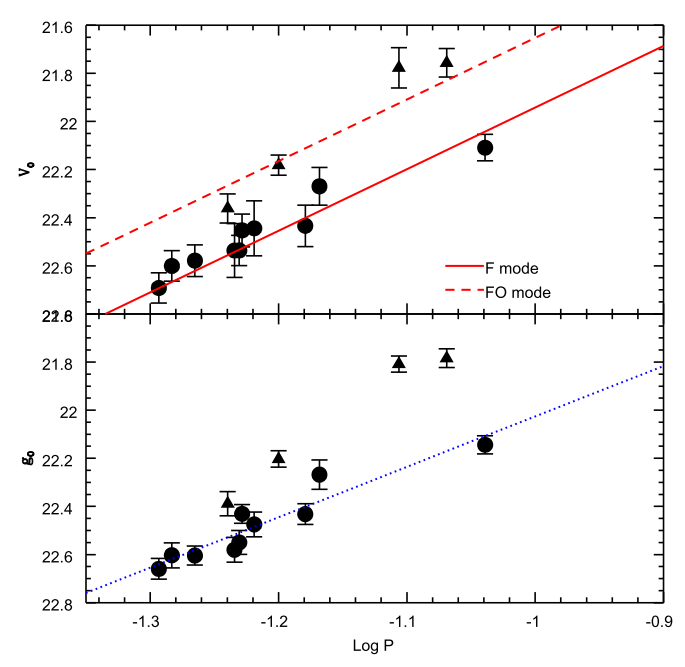


Figure 13. (Top) Extinction-corrected V magnitude (transformed from our g and r) vs. the logarithm of the pulsation period for the 14 DC stars found in Sextans. The red lines correspond to the PLZ relationships given by Nemec et al. (1994) for F and FO pulsators shifted by the distance modulus found with the RR Lyrae stars, $\mu_0 = 19.64$, and assuming $[\text{Fe/H}]_{\text{ref}} = -1.93$ dex. Based on these relationships, the stars identified with triangles were associated with the FO mode. (Bottom) Extinction-corrected g magnitude vs. the logarithm of the pulsation period. The dotted blue line is a fit to the alleged F-mode pulsating stars (see text).

stars were observed only in the g band, we will assume the distance modulus from that band in the following analysis.

6. The PL Relationship of DC Stars in Sextans

A plot of the extinction-corrected *g* magnitude, *g*₀, versus the logarithm of the period (bottom panel in Figure 13) of the 14 DC stars in Sextans shows a clear trend, with the shorter-period variables being fainter than the ones with longer periods. There is a lot of scatter in the data, though, likely due to the fact that our sample may contain stars pulsating in different modes. As discussed before (Section 3.1), there is no unambiguous way to recognize a fundamental (F) mode pulsator from a first overtone (FO) one with the data at hand, and different pulsation modes obey different PLZ relationships (e.g., Nemec et al. 1994).

Since the distance to Sextans has been set by the RR Lyrae stars, we can use the known PLZ relationships of DC stars to infer their pulsation mode. Nemec et al. (1994) derived such relationships but in the Johnson V band. Thus, we transformed our mean g and r magnitudes (in the PS1 system) of the DC stars in Sextans to V using

$$V = g + 0.006 - 0.525 * (g - r)$$
 (3)

from Tonry et al. (2012). The extinction-corrected V_0 magnitudes (obtained using Schlafly & Finkbeiner 2011) versus the logarithm period are shown in the top panel of Figure 13, which also shows both the F and FO relationships from Nemec et al. (1994) shifted to a distance modulus of 19.64 mag (from the RR Lyrae stars) and assuming [Fe/H] = -1.93 dex. The agreement of those relationships with our data is very good, and we can infer from there that there are four

Table 5
Known DC Stars in Extragalactic Systems

| Galaxy | N_{DC} | Mean Period (day) | References |
|----------------|----------|----------------------|--|
| | | Classical Sate | ellites |
| LMC | 2323 | 0.074 | Garg et al. (2010; SuperMACHO) |
| | 1276 | 0.110 | Poleski et al. (2010; OGLE-III) ^a |
| Fornax | 85 | 0.070 | Poretti et al. (2008) |
| Carina | 426 | 0.060 | Vivas & Mateo (2013); Coppola et al. (2015) ^b |
| Sculptor | 23 | 0.066 | Martínez-Vázquez et al. (2016) |
| Sagittarius | 3 | 0.0481 | Pych et al. (2001) ^c |
| Sextans | 14 | 0.065 | This work |
| | | UFD Satell | ites |
| Leo IV | 1 | 0.099 | Moretti et al. (2009) |
| Coma Berenices | 1 | 0.125 | Musella et al. (2009) |

Notes.

stars pulsating in the FO mode. These stars are indicated with triangles in Figure 13. Assuming that the remaining 10 stars are then F pulsators, we obtain, via least-squares fitting, the following relationships for Sextans:

$$V_0 = -2.22 \log P + 19.77$$
; rms = 0.04, (4)

$$g_0 = -2.10 \log P + 19.93$$
; rms = 0.05. (5)

Anchoring these equations to the distance modulus given by the RR Lyrae stars, the PL relationships for Sextans (F-mode) DC stars are

$$M_V = -2.10\log P + 0.13\tag{6}$$

and

$$M_g = -2.01 \log P + 0.29. \tag{7}$$

The resulting slope in our V–PL relationship is, within the errors, compatible with the one provided by Nemec et al. (1994; -2.56 ± 0.54). Surprisingly, the slope is somewhat shallower than the slopes given by Poretti et al. (2008), McNamara (2011), Cohen & Sarajedini (2012), and Fiorentino et al. (2015). The slope of the PL in Carina (Vivas & Mateo 2013), however, is even shallower (-1.68). These apparent discrepancies between different works demonstrate the need to continue gathering data of DC stars in other systems in order to study the effects of local conditions (age, metallicity, star formation history) in the PL relationship.

7. The DC Population in Sextans and Other Galaxies

To date, DC stars have been searched for and found in six of the "classical" satellites of the Milky Way, including this work, and two ultrafaint dwarf (UFD) satellites. The number and mean period of the DC population in those systems are summarized in Table 5. The search in Sagittarius, however, is incomplete, since no dedicated survey in this galaxy has been done. The three stars listed in Table 5 refer to stars

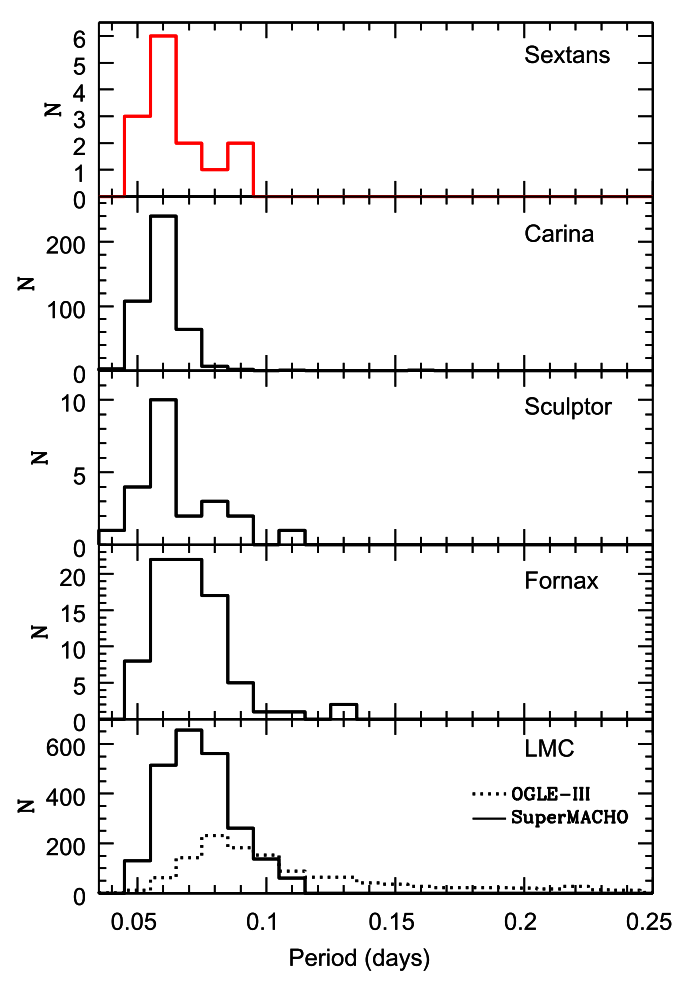


Figure 14. Period distribution of DC stars in the five classical satellites with known DC stars. References for each galaxy are given in Table 5.

serendipitously discovered in the background of the M55 globular cluster.

In Figure 14, we show the period distribution of the DC stars in the five satellite galaxies with a large number of known DC stars. We do not include either Leo IV or Coma Berenices because they have only one star each (see Table 5). The figure includes DC stars in the LMC from two different experiments: OGLE-III (Poleski et al. 2010) and SuperMACHO (Garg et al. 2010). The period distribution is quite different among those two samples, so we show them separately. The DC stars in the SuperMACHO sample (Garg et al. 2010) have a mean period of 0.074 day, and the distribution is not much different from that of Fornax, which has a mean period of 0.07 day. On the other hand, Poleski et al. (2010) showed a much wider period distribution among the DC stars measured by OGLE-III, with a long tail toward long periods, which is not observed in any of the other data sets. The DC stars in Sextans have a very similar mean period to the ones in Sculptor (Martínez-Vázquez et al. 2016). Like Sculptor, the distribution shows a peak at $\sim 0.055 \,\mathrm{day}$ but has a tail toward longer periods. None of these two galaxies have stars with periods longer than 0.12 day. Carina's sample also peaks at the same period, but the distribution is more symmetrical, with no extension toward longer periods. Surprisingly, the two DC stars in the UFD galaxies have significantly longer periods (0.099 and 0.125 day) than the mean of the other galaxies. To search for

^a The original OGLE-III catalog contains 2786 stars, but we are not including here either stars flagged as uncertain or Galactic stars based on proper motions (Poleski et al. 2010).

^b Both catalogs were merged, and duplicates were eliminated.

^c In the background of the M55 globular cluster.

DC stars in other UFDs will be interesting in order to confirm this trend.

The Sextans population of variables is not much different from that of Sculptor. Sextans has 14 DC stars and 227 RR Lyrae stars. On the other hand, from Martínez-Vázquez et al. (2016), Sculptor has 23 DC stars and 523 RR Lyrae stars. The ratio of DC stars to RR Lyrae stars is then 1:16 and 1:22 in Sextans and Sculptor, respectively. On the contrary, the ratio is ~1:1 in Fornax (Poretti et al. 2008), and Carina stands significantly apart from these other galaxies in having a ratio of 5:1, meaning that it contains more DC than RR stars. Both Sextans and Sculptor are galaxies that are dominated by an old population with only small contributions from younger stellar populations, which is not the case for the other classical dwarfs in Table 5.

8. Summary and Conclusions

A full survey of Sextans had been difficult in the past due to its large extension in the sky and distance from the Sun. The combination of the large FoV of DECam with a 4 m telescope allowed us to search for variable stars in the instability strip of the Sextans dSph galaxy down to magnitude $g \sim 23$. The survey, covering 7 deg², covers a large part of the galaxy. Although the true size of Sextans is controversial, if the smallscale tidal radius by Roderick et al. (2016) is confirmed, this will be the first time that a full census of pulsating variable stars is done in the whole galaxy. We found seven anomalous Cepheids, 197 RR Lyrae stars, and 14 DCs. In addition, there are four stars with properties of either RR Lyrae stars or DCs but in a location within the CMD that suggests that they are instead Milky Way foreground stars. In this paper, we focused on two aspects of the survey: (i) the spatial distribution of the variable stars and (ii) the properties of the DC population.

Variable stars have been used in the past to trace extratidal material in stellar systems. For example, one of the first hints of the existence of long tidal tails coming from the Sagittarius dwarf came indeed from RR Lyrae stars (Mateo et al. 1996; Vivas et al. 2001). Extratidal variable stars have also been found in Carina (Vivas & Mateo 2013), Hercules (Garling et al. 2018), and Tucana III (C. Martínez-Vázquez et al. 2018, in preparation). Our survey extends beyond the Roderick et al. (2016) tidal radius of Sextans along the direction of the semimajor axis and provides an opportunity to trace any possible sign of debris outside the tidal radius. Indeed, we found two RR Lyrae stars and one anomalous Cepheid outside the tidal radius of Sextans. Not only are these stars located in the right place in the CMD to be considered Sextans members, they also have Gaia proper motions consistent with the bulk of the Sextans population. There is an additional extratidal RR Lyrae star in the LSQ survey that is just outside our footprint. A very rough estimate of the amount of tidal debris can be obtained, considering there are three extratidal RR Lyrae stars out of a total of 227 (including the ones from other surveys that we missed due to the CCD gaps). This suggests a minimum of 1% of material outside the tidal radius. This is just a lower limit, because our survey does not cover regions outside Sextans along the semiminor axis; thus, if the extratidal material is more uniformly distributed, we can be missing part of it. If Sextans is larger, as suggested by Irwin & Hatzidimitriou (1995), Okamoto et al. (2017), and Cicuéndez et al. (2018), all variable stars are inside the tidal radius. In that

case, our survey does not have enough coverage to study if extratidal material indeed exists.

In an analysis of the stellar populations of Sextans, also done with DECam, by Roderick et al. (2016), the authors concluded that the BS population is more centrally concentrated that the blue HB population, which suggests that most of the BS stars may be main-sequence stars from an intermediate-age population. The specific star formation history of Sextans may be responsible for such a population gradient (Lee et al. 2009). We find support for this scenario with our variable stars. The RR Lyrae stars, an unequivocal old-age tracer, are more widely distributed than the DC population, which are variable BS stars. No DC stars were found in the external part of Sextans. An interesting additional puzzle comes from the anomalous Cepheid stars. There is at least one extratidal anomalous Cepheid in Sextans, but there is a possibility that two stars that we classified originally as foreground RR Lyrae stars are indeed anomalous Cepheids, in which case, they would also be extratidal stars. Anomalous Cepheids are usually regarded as an intermediate-age population, but they do not have the same spatial distribution as the DC stars. A possible explanation for this apparent discrepancy may come from the idea that some anomalous Cepheids are produced through binary evolution (Gautschy & Saio 2017), in this case, of old stars.

The second aspect on which we focused in this paper was the DC population. With the DC stars found in Sextans, there are now five Local Group galaxies that have been adequately surveyed for this type of star: the LMC, Fornax, Carina, Sculptor, and Sextans. These galaxies cover a wide range of properties and different star formation histories. The DC population seems to change accordingly. Sextans and Sculptor, two galaxies dominated by an old population, have relatively few DC stars. The RR Lyrae variables dominate the number of pulsating variables in those galaxies. On the contrary, galaxies with a strong young and intermediate-age population have a rich population of DC stars; in the case of Carina, for example, there are several times more DC than RR Lyrae stars. The increased census of known DC stars in these different systems provides constraints on the models of production of DC stars under different environmental conditions.

The increased census is also useful to investigate the use and limitations of DC stars as standard candles. In this work, we set a PL relationship that is anchored to the distance modulus obtained by the RR Lyrae stars. The resulting PL relationship has a dispersion of only 0.04 mag. In the future, we plan to explore the possibility that a metallicity-independent PL relationship like the one obtained by Cohen & Sarajedini (2012) with data from only a few galaxies can be used globally.

Sextans has a rich population of RR Lyrae stars compared with its DC population. It is clear, then, that RR Lyrae stars would be the ideal choice for standard candles in this galaxy. They are not only more numerous but also brighter than DC stars. However, RR Lyrae stars are not necessarily as abundant in other systems. Carina (Vivas & Mateo 2013; Coppola et al. 2015) has more DC stars than RR Lyrae stars. Leo T (Clementini et al. 2012) has only one RR Lyrae star but several anomalous Cepheids. Just recently, a very young, disrupting open cluster was discovered in the Milky Way's halo (Price-Whelan et al. 2018); given its young age, this system presumably does not have RR Lyrae stars. These examples illustrate the importance of setting up alternative standard candles that trace different stellar populations. The DC

stars will be observed by LSST to large distances and will potentially provide a tool to study halo substructures and stellar populations to very large distances in the Galactic halo.

We thank the anonymous referee for an insightful review of this manuscript. We thank Marcio Catelan and Pía Amigo for providing us with Amigo's (2012) PhD thesis manuscript, which contains the full table of variable stars in Sextans detected in her work. J.A.-G. acknowledges support by FONDECYT Iniciacin 11150916 and the Ministry of Economy, Development, and Tourism's Millennium Science Initiative through grant IC120009, awarded to the Millennium Institute of Astrophysics (MAS). M.M. acknowledges support from NSF grants AST-1312997 and AST-1815403.

This project used data obtained with the Dark Energy Camera (DECam), which was constructed by the Dark Energy Survey (DES) collaboration. Funding for the DES projects has been provided by the U.S. Department of Energy, the U.S. National Science Foundation, the Ministry of Science and Education of Spain, the Science and Technology Facilities Council of the United Kingdom, the Higher Education Funding Council for England, the National Center for Supercomputing Applications at the University of Illinois at Urbana-Champaign, the Kavli Institute of Cosmological Physics at the University of Chicago, the Center for Cosmology and Astro-Particle Physics at the Ohio State University, the Mitchell Institute for Fundamental Physics and Astronomy at Texas A&M University, Financiadora de Estudos e Projetos, Fundação Carlos Chagas Filho de Amparo à Pesquisa do Estado do Rio de Janeiro, Conselho Nacional de Desenvolvimento Científico e Tecnológico and the Ministério da Ciência, Tecnologia e Inovação, the Deutsche Forschungsgemeinschaft, and the Collaborating Institutions in the Dark Energy Survey. The Collaborating Institutions are Argonne National Laboratory, the University of California at Santa Cruz, the University of Cambridge, Centro de Investigaciones Enérgeticas, Medioambientales y Tecnológicas-Madrid, the University of Chicago, University College London, the DES-Brazil Consortium, the University of Edinburgh, the Eidgenössische Technische Hochschule (ETH) Zürich, Fermi National Accelerator Laboratory, the University of Illinois at Urbana-Champaign, the Institut de Ciències de l'Espai (IEEC/CSIC), the Institut de Física d'Altes Energies, Lawrence Berkeley National Laboratory, the Ludwig-Maximilians Universität München and the associated Excellence Cluster Universe, the University of Michigan, the National Optical Astronomy Observatory, the University of Nottingham, Ohio State University, the OzDES Membership Consortium, the University of Pennsylvania, the University of Portsmouth, SLAC National Accelerator Laboratory, Stanford University, the University of Sussex, and Texas A&M University.

Based on observations at Cerro Tololo Inter-American Observatory, National Optical Astronomy Observatory (NOAO Prop. IDs: 2014A-0313, 2017A-0951; PI: Vivas), which is operated by the Association of Universities for Research in Astronomy (AURA) under a cooperative agreement with the National Science Foundation.

The Pan-STARRS1 Surveys (PS1) and the PS1 public science archive have been made possible through contributions by the Institute for Astronomy; the University of Hawaii; the Pan-STARRS Project Office; the Max Planck Society and its participating institutes, the Max Planck Institute for Astronomy, Heidelberg, and the Max Planck Institute for Extraterrestrial

Physics, Garching; Johns Hopkins University; Durham University; the University of Edinburgh; Queen's University Belfast; the Harvard-Smithsonian Center for Astrophysics; the Las Cumbres Observatory Global Telescope Network Incorporated; the National Central University of Taiwan; the Space Telescope Science Institute; the National Aeronautics and Space Administration under grant No. NNX08AR22G, issued through the Planetary Science Division of the NASA Science Mission Directorate; National Science Foundation grant No. AST-1238877; the University of Maryland; Eotvos Lorand University (ELTE); Los Alamos National Laboratory; and the Gordon and Betty Moore Foundation.

This work has made use of data from the European Space Agency (ESA) mission *Gaia* (https://www.cosmos.esa.int/gaia), processed by the *Gaia* Data Processing and Analysis Consortium (DPAC; https://www.cosmos.esa.int/web/gaia/dpac/consortium). Funding for the DPAC has been provided by national institutions, in particular the institutions participating in the *Gaia* Multilateral Agreement.

Facility: Blanco (DECam).

ORCID iDs

A. Katherina Vivas https://orcid.org/0000-0003-4341-6172 Javier Alonso-García https://orcid.org/0000-0003-3496-3772

Alistair Walker https://orcid.org/0000-0002-7123-8943

References

```
Alonso-García, J., Mateo, M., Sen, B., et al. 2012, AJ, 143, 70
Amigo, P. 2012, PhD thesis, Pontificia Universidad Católica de Chile
Balona, L. A., & Nemec, J. M. 2012, MNRAS, 426, 2413
Battaglia, G., Tolstoy, E., Helmi, A., et al. 2011, MNRAS, 411, 1013
Breger, M. 2000, in ASP Conf. Ser. 210, Delta Scuti and Related Stars, ed.
   M. Breger & M. Montgomery (San Francisco, CA: ASP), 3
Catelan, M., & Smith, H. A. 2015, Pulsating Stars (New York: Wiley)
Cicuéndez, L., Battaglia, G., Irwin, M., et al. 2018, A&A, 609, A53
Clementini, G. 2014, in IAU Symp. 301, Precision Asteroseismology, ed.
   J. A. Guzik et al. (Cambridge: Cambridge Univ. Press), 129
Clementini, G., Cignoni, M., Contreras Ramos, R., et al. 2012, ApJ, 756, 108
Cohen, R. E., & Sarajedini, A. 2012, MNRAS, 419, 342
Coppola, G., Marconi, M., Stetson, P. B., et al. 2015, ApJ, 814, 71
Fiorentino, G., Marconi, M., Bono, G., et al. 2015, ApJ, 810, 15
Fiorentino, G., & Monelli, M. 2012, A&A, 540, A102
Flaugher, B., Diehl, H. T., Honscheid, K., et al. 2015, AJ, 150, 150
Förster, F., Maureira, J. C., San Martín, J., et al. 2016, ApJ, 832, 155
Gaia Collaboration, Brown, A. G. A., Vallenari, A., et al. 2018a, A&A,
Gaia Collaboration, Helmi, A., van Leeuwen, F., et al. 2018b, A&A, 616, A12
Gaia Collaboration, Prusti, T., de Bruijne, J. H. J., et al. 2016, A&A, 595, A1
Garg, A., Cook, K. H., Nikolaev, S., et al. 2010, AJ, 140, 328
Garling, C., Willman, B., Sand, D. J., et al. 2018, ApJ, 852, 44
Gautschy, A., & Saio, H. 2017, MNRAS, 468, 4419
Irwin, M., & Hatzidimitriou, D. 1995, MNRAS, 277, 1354
Irwin, M. J., Bunclark, P. S., Bridgeland, M. T., & McMahon, R. G. 1990,
  MNRAS, 244, 16P
Kirby, E. N., Martin, C. L., & Finlator, K. 2011, ApJL, 742, L25
Lafler, J., & Kinman, T. D. 1965, ApJS, 11, 216
Lee, M. G., Park, H. S., Park, J.-H., et al. 2003, AJ, 126, 2840
Lee, M. G., Yuk, I.-S., Park, H. S., Harris, J., & Zaritsky, D. 2009, ApJ,
   703, 692
Magnier, E. A., Schlafly, E. F., Finkbeiner, D. P., et al. 2016, arXiv:1612.
  05242
Maintz, G., & de Boer, K. S. 2005, A&A, 442, 229
Martínez-Vázquez, C. E., Stetson, P. B., Monelli, M., et al. 2016, MNRAS,
   462, 4349
Mateo, M. 1993, in ASP Conf. Ser. 53, Blue Stragglers, ed. R. A. Saffer (San
  Francisco, CA: ASP), 74
Mateo, M., Fischer, P., & Krzeminski, W. 1995, AJ, 110, 2166
```

Mateo, M., Mirabal, N., Udalski, A., et al. 1996, ApJL, 458, L13

```
Mateo, M., Nemec, J., Irwin, M., & McMahon, R. 1991, AJ, 101, 892
McNamara, D. H. 2011, AJ, 142, 110
Medina, G. E., Muñoz, R. R., Vivas, A. K., et al. 2018, ApJ, 855, 43
Moretti, M. I., Dall'Ora, M., Ripepi, V., et al. 2009, ApJL, 699, L125
Musella, I., Ripepi, V., Clementini, G., et al. 2009, ApJL, 695, L83
Nemec, J. M., Nemec, A. F. L., & Lutz, T. E. 1994, AJ, 108, 222
Okamoto, S., Arimoto, N., Tolstoy, E., et al. 2017, MNRAS, 467, 208
Poleski, R., Soszyński, I., Udalski, A., et al. 2010, AcA, 60, 1
Poretti, E., Clementini, G., Held, E. V., et al. 2008, ApJ, 685, 947
Price-Whelan, A. M., Nidever, D. L., Choi, Y., et al. 2018, arXiv:1811.05991
Pych, W., Kaluzny, J., Krzeminski, W., Schwarzenberg-Czerny, A., &
  Thompson, I. B. 2001, A&A, 367, 148
Roderick, T. A., Jerjen, H., Da Costa, G. S., & Mackey, A. D. 2016, MNRAS,
Saha, A., & Hoessel, J. G. 1990, AJ, 99, 97
Samus, N. N., Kazarovets, E. V., Durlevich, O. V., Kireeva, N. N., &
   Pastukhova, E. N. 2017, ARep, 61, 80
```

```
Sandage, A., & Tammann, G. A. 2006, ARA&A, 44, 93
Schechter, P. L., Mateo, M., & Saha, A. 1993, PASP, 105, 1342
Schlafly, E. F., & Finkbeiner, D. P. 2011, ApJ, 737, 103
Schlegel, D. J., Finkbeiner, D. P., & Davis, M. 1998, ApJ, 500, 525
Sesar, B., Ivezić, Ž., Grammer, S. H., et al. 2010, ApJ, 708, 717
Sesar, B., Hernitschek, N., Mitrović, S., et al. 2017, AJ, 153, 204
Skarka, M. 2014, MNRAS, 445, 1584
Stetson, P. B., Fiorentino, G., Bono, G., et al. 2014, PASP, 126, 616
Taylor, M. B. 2006, in ASP Conf. Ser. 351, Astronomical Data Analysis Software
and Systems XV, ed. C. Gabriel et al. (San Francisco, CA: ASP), 666
Tonry, J. L., Stubbs, C. W., Lykke, K. R., et al. 2012, ApJ, 750, 99
Valdes, F., Gruendl, R. & DES Project 2014, in ASP Conf. Ser. 485,
   Astronomical Data Analysis Software and Systems XXIII, ed. N. Manset &
   P. Forshay (San Francisco, CA: ASP), 379
Vivas, A. K., & Mateo, M. 2013, AJ, 146, 141
Vivas, A. K., Zinn, R., Andrews, P., et al. 2001, ApJL, 554, L33
Zinn, R., Horowitz, B., Vivas, A. K., et al. 2014, ApJ, 781, 22
```